View Article Online / Journal Homepage / Table of Contents for this issue

Theory of nitride oxide adsorption on transition metal (111) surfaces: a first-principles investigation

Zhen-Hua Zeng,[ac] Juarez L. F. Da Silva[b] and Wei-Xue Li*[a]

Received 6th October 2009, Accepted 18th December 2009
First published as an Advance Article on the web 26th January 2010
DOI: 10.1039/b920857g

Downloaded by Dalian Institute of Chemical Physics, CAS on 02/05/2013 07:43:48.
Published on 26 January 2010 on http://pubs.rsc.org | doi:10.1039/B920857G

In this work, we report a density functional theory study of nitric oxide (NO) adsorption on close-packed transition metal (TM) Rh(111), Ir(111), Pd(111) and Pt(111) surfaces in terms of adsorption sites, binding mechanism and charge transfer at a coverage of Θ_{NO} = 0.25, 0.50, 0.75 monolayer (ML). Based on our study, an unified picture for the interaction between NO and TM(111) and site preference is established, and valuable insights are obtained. At low coverage (0.25 ML), we find that the interaction of NO/TM(111) is determined by an electron donation and back-donation process *via* the interplay between NO 5σ/2π* and TM d-bands. The extent of the donation and back-donation depends critically on the coordination number (adsorption sites) and TM d-band filling, and plays an essential role for NO adsorption on TM surfaces. DFT calculations shows that for TMs with high d-band filling such as Pd and Pt, hollow-site NO is energetically the most favorable, and top-site NO prefers to tilt away from the normal direction. While for TMs with low d-band filling (Rh and Ir), top-site NO perpendicular to the surfaces is energetically most favorable. Electronic structure analysis show that irrespective of the TM and adsorption site, there is a net charge transfer from the substrate to the adsorbate due to overwhelming back-donation from the TM substrate to the adsorbed NO molecules. The adsorption-induced change of the work function with respect to bare surfaces and dipole moment is however site dependent, and the work function increases for hollow-site NO, but decreases for top-site NO, because of differences in the charge redistribution. The interplay between the energetics, lateral interaction and charge transfer, which is element dependent, rationalizes the structural evolution of NO adsorption on TM(111) surfaces in the submonolayer regime.

1. Introduction

The catalytic reduction of NO_x species is one of the most important reactions that takes place in the three-way-catalysts (TWCs), which are used to convert pollutants from combustion exhausts to environmentally friendly substances.[1] Among others, transition metal (TM) particles of rhodium, palladium and platinum supported on oxides are the main components of automotive TWC devices.[2] In addition, iridium is also being considered for the improvement of TWCs devices due to its ability to decompose NO and reduce NO_x with hydrocarbons.[3,4] The study of the interaction of NO_x species with those particles is of technological importance to improve the catalytic activities of current catalytic devices and rationalize the design of new catalysts with better stability and economic efficiency. As a matter of fact, identification of the adsorption structures, site preference as well as bonding strength of NO on Rh, Pd, Ir, and Pt surfaces at the microscopic scale are essential. As a model system, NO adsorption on Rh(111), Pd(111), Ir(111), and Pt(111) surfaces has been studied extensively by experimental[5–24] and theoretical[12,14,24–36] techniques, and valuable insights have been obtained. Nevertheless, as described below, even for these well studied model systems, a generic understanding of NO adsorption on TMs is lacking, and in some cases even controversial, and we address this using density functional theory (DFT) calculations in this work.

For NO adsorption on Rh(111), experimental studies[6–9] have proposed that NO adsorbs preferentially in fcc (noted as F) sites at coverage (Θ_{NO}) of less than 0.25 monolayer (ML), populates top sites for $0.25 < \Theta_{NO} < 0.50$, and NO forms a $p(2 \times 2)$-3NO(fcc + hcp + top) (noted as FHT) at 0.75 ML. A temperature-programmed desorption (TPD) study[8] reported that with increasing temperature, NO in the top sites desorbs first, at 395 K, and fcc and hcp hollow-sites NO desorb at 490 K. This indicated that NO adsorbed in the top-site has the weakest bonding with respect to the substrates, as expected since as the top sites are populated by NO only at high coverages. In addition, DFT calculations found that NO adsorbs preferentially in the hcp sites at low coverage instead of the fcc sites suggested by experiments,[6–9] and the $c(4 \times 2)$-2NO(*FH*) and $p(2 \times 2)$-3NO(FHT) structures are energetically the most favorable at 0.50 and 0.75 ML, respectively.[12,25–28]

For NO adsorption on Pd(111), both experimental and theoretical investigations[10–14,27,28] reported a consistent

[a] *State Key Laboratory of Catalysis and Center for Theoretical and Computational Chemistry, Dalian Institute of Chemical Physics, Chinese Academy of Sciences, 116023 Dalian, China. E-mail: wxli@dicp.ac.cn*
[b] *Instituto de Física de São Carlos, Universidade de São Paulo, Caixa Postal 369, 13560-970 SP, São Carlos, Brazil*
[c] *Graduate School of the Chinese Academy of Sciences, 100039 Beijing, China*

Downloaded by Dalian Institute of Chemical Physics, CAS on 02/05/2013 07:43:48.
Published on 26 January 2010 on http://pubs.rsc.org | doi:10.1039/B920857G

picture for the adsorbate structures, namely, $p(2 \times 2)$-NO(fcc) at 0.25 ML, $c(4 \times 2)$-2NO(*FH*) at 0.50 ML, and $p(2 \times 2)$-3NO(FHT) at 0.75 ML. A recent low-energy electron diffraction (LEED) study at 245 K[10] found that the hollow-site NO, which was perpendicular to the surfaces at 0.25 ML, became tilted at higher coverage. Whether the driving force for the tilting comes from the lateral repulsion or thermal effects is however unclear.

For NO/Ir(111), Fujitani *et al.* reported that NO adsorbs on the top sites at low coverage, and populates the fcc hollow sites with increase of coverage.[15] This is in contrast to the available theoretical results,[29] in which the hcp hollow-site NO molecules were predicted to be favorable sites after NO adsorption at the top sites.

For NO/Pt(111), a consistent picture of the adsorption structures has been reported by both experimental and theoretical investigations,[16–23,28,30–36] and is summarised as follows: $p(2 \times 2)$-NO(F) forms at 0.25 ML, $p(2 \times 2)$-2NO(FT) at 0.5 ML, and $p(2 \times 2)$-3NO(FHT) at 0.75 ML. In this context, we note that the measured zero N 1s level shift of adsorbed NO at different sites (fcc and top) remained a puzzle, as discussed in detail in a recent theoretical study.[36]

The brief survey above shows clearly that the interaction between NO and TMs depends sensitively on the sites, coverage and TMs involved. To reveal the physics underlying the adsorption of NO on TM(111) surfaces, we report in this work a first-principles study based on DFT calculation of NO adsorption on Rh(111), Pd(111), Ir(111), and Pt(111) surfaces in the submonolayer regime of 0.25, 0.50, and 0.75 ML, respectively. Among the four TMs considered, two elements (Rh and Pd) are 4d elements, and the remaining two (Ir and Pt) are 5d elements. In addition, these four TMs have different d-fillings. The comparative study for NO adsorption on these surfaces provides therefore an excellent insight into the mechanism between NO and the corresponding TMs.

2. Computational methods

Self-consistent total energy calculations were performed based on the all-electron projected augmented wave (PAW) method[37,38] and DFT[39,40] within the generalized gradient approximation (GGA) formulated by Perdew, Burke, and Ernzehof (PBE)[41] as implemented in the Vienna *Ab initio* Simulation Package (VASP).[42,43] The PAW projectors provided in VASP were employed, and a cutoff energy of 400 eV was used for the plane-wave expansion for all calculations. For bulk calculations, Brillouin zone integration of $(12 \times 12 \times 12)$ Monkhorst–Pack **k**-point grids[44] were used, while for the surface calculations, Γ-point centered grids of $(6 \times 6 \times 1)$ and $(7 \times 6 \times 1)$ were used for the $p(2 \times 2)$ and $c(4 \times 2)$ structures. For free NO molecules, we employed an orthorhombic box ($15 \times 15.5 \times 16$ Å^3) and a single **k**-point (0.25,0.25,0.25) for the Brillouin zone sampling. We employ a Fermi function with a temperature broadening parameter of $k_BT = 0.15$ eV (k_B is the Boltzmann constant) to improve the convergence, and the resulted total energies are extrapolated to zero temperature to calculate the energetics.

All surface calculations were performed using the theoretical bulk equilibrium lattice constant of Rh, Pd, Ir, and Pt in the face-centered cubic structure, *i.e.*, a_0 = 3.84, 3.95, 3.88, and 3.98 Å for Rh, Pd, Ir and Pt, which are 1.1, 1.6, 1.0 and 1.5% larger than the experimental values, respectively.[45] The surfaces were modeled employing the repeated slab geometry composed of 4 layers in the slab and a vacuum region of about 11 Å, in which NO was adsorbed on one side of the slab. The NO molecules and the topmost two layers were relaxed during structure optimization until the residual forces on the atoms were less than 0.02 eV Å^{-1}. Previous calculations using a thicker (seven layers) and symmetric slab with NO adsorbed on both sides showed that both slabs give the same adsorption energy and work function sequence for NO adsorption at different sites with absolute energy difference less than 50 meV.[36]

Experimental studies have observed the formation of $p(2 \times 2)$ or $c(4 \times 2)$ ordered structures for NO adsorption on Rh(111), Pd(111) and Pt(111), as defined in Figs. 1 and 2, and considered in present work. Calculations were performed for Θ_{NO} = 0.25, 0.50 and 0.75 ML, in which NO molecules

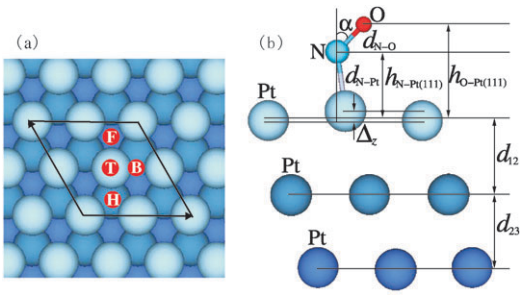

Fig. 1 (a) The possible adsorption sites fcc(F), hcp(H), top(T), bridge(B) in the $p(2 \times 2)$ unit cell. (b) Side view of NO/TM(111) for NO in the top sites, for which the geometric parameters are defined and listed in Table 3.

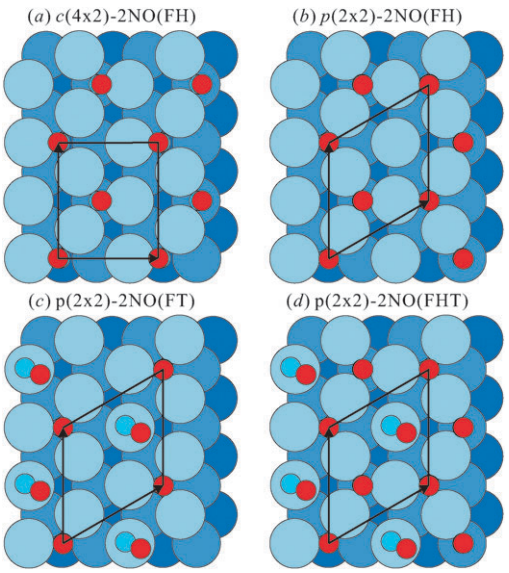

Fig. 2 Schematic top view of the various structures formed for NO on TM(111) surfaces: (a) $c(4 \times 2)$-2NO(*FH*), (b) $p(2 \times 2)$-2NO(FH), (c) $p(2 \times 2)$-2NO(FT) at 0.50 ML, and (d) $p(2 \times 2)$-2NO(FHT) at 0.75 ML, respectively.

 This journal is © the Owner Societies 2010

Downloaded by Dalian Institute of Chemical Physics, CAS on 02/05/2013 07:43:48.
Published on 26 January 2010 on http://pubs.rsc.org | doi:10.1039/B920857G

are initially placed at the high-symmetry sites, namely, fcc (F), hcp (H), top (T), and bridge (B) at a coverage of 0.25 ML, as well as the combinations of different adsorption sites, fcc + hcp (FH), fcc + top (FT), hcp + top (HT) and fcc + hcp + top (FHT) at higher coverages. No symmetry constraints were applied during the geometric optimizations to escape from possible local minima.

3. Results

3.1 Clean surfaces

The calculated interlayer relaxations of the topmost layers, Δd_{12} and Δd_{23}, and surface work functions, Φ, are given in Table 1. Test calculations showed that the results were essentially the same by using different shape unit cells (hexagonal $p(2 \times 2)$ and rectangular $c(4 \times 2)$), which indicates a good convergence of the present setup. Compared with the bulk truncated interlayer spacing, we found a modest contraction of both d_{12} and d_{23} for Rh(111) and Ir(111), while a slight expansion of d_{12} and a contraction of d_{23} for Pd(111) and Pt(111). Considering possible quantum size effects,[64] they are in good agreement with previous calculations, and the agreement with available experiments is also reasonable good. Calculated Φ values are 5.13, 5.27, 5.45 and 5.73 eV for Rh(111), Pd(111), Ir(111) and Pt(111), respectively. Compared to previous DFT-GGA calculations,[47–50,57] the difference is less than 0.12 eV. The agreement with experiment are satisfactory, taking into account the uncertainties in the measurements.[58–63]

Table 1 The calculated variation of interlayer spacing with respect to bulk truncated values (%) and surface work functions (in eV) of clean transition metal surfaces. The available experimental and theoretical results in literature are given for comparison

		Rh(111)	Pd(111)	Ir(111)	Pt(111)
Δd_{12}	Calc.[a]	−1.52	0.16	−1.94	0.33
	Calc.	−1.5[b]	−0.01[c]	—	+1.14[c]
	Calc.	−1.8[d]	−0.1[e]	—	+1.2[f]
	Exp.	−1.4 ± 0.9[g]	1.3 ± 1.3[h]	−1.2[i]	+0.9[j]
	Exp.	−0.9 ± 0.9[k]	2.4 ± 0.9[l]	—	+1.0 ± 0.1[m]
Δd_{23}	Calc.[a]	−1.02	−0.56	−1.76	−1.03
	Calc.	−1.0[b]	−0.41[c]	—	−0.29[c]
	Calc.	−0.9[d]	+0.1[e]	—	−0.5[f]
	Exp.	−1.4 ± 1.8[g]	1.3 ± 1.3[h]	−0.6[i]	−0.29[j]
	Exp.	−0.0 ± 0.9[k]	0.7 ± 0.9[l]	—	—
Φ	Calc.[a]	5.13	5.27	5.45	5.73
	Calc.	5.10[n]	5.30[n]	5.55[n]	5.85[n]
	Calc.	5.23[d]	5.25[e]	—	5.7[f]
	Calc.	—	5.22[d]	—	5.69[c]
	Exp.	4.98[o]	5.6[o]	5.76[o]	5.7[o]
	Exp.	5.3[p]	5.6[q]	—	5.7 ± 0.2[r]
	Exp.	—	5.55[s]	—	6.1[t]

[a] This work, DFT-PBE using PAW method. [b] ref. 46, DFT-PBE using pseudopotential method. [c] ref. 47, DFT-PBE using FP-LAPW method. [d] ref. 48, DFT-PBE using FP-LAPW method. [e] ref. 49, DFT-PBE using FP-LAPW method. [f] ref. 50, DFT-PBE using pseudopotential method. [g] ref. 51, LEED. [h] ref. 52, LEED. [i] ref. 53, surface X-ray diffraction (SXRD). [j] ref. 21, LEED. [k] ref. 54, LEED. [l] ref. 55, LEED. [m] ref. 56, LEED. [n] ref. 57, DFT-PW91 using PAW method. [o] ref. 58, (111) surface for Pd, Ir and Pt, polycrystalline for Rh. Photoelectron spectroscopy (PES) method. [p] ref. 59, PES method. [q] ref. 60, PES method. [r] ref. 61, PES, method. [s] ref. 62, Kelvin method. [t] ref. 63, PES method.

3.2 Adsorption energies

The average adsorption energy of NO on the surfaces, E_{ad}, was calculated using,

$$E_{ad} = (E_{tot}^{NO/TM(111)} - E_{tot}^{TM(111)} - N \times E_{tot}^{NO})/N, \qquad (1)$$

where $E_{tot}^{NOTM(111)}$, $E_{tot}^{TM(111)}$, and E_{tot}^{NO} are the total energies of NO/TM(111), clean TM(111), and NO in the gas phase, respectively and N is the number of adsorbed NO molecules in the unit cell. The results are shown in Figs. 3 and 4, and tabulated in Table 2.

For NO adsorption at 0.25 ML, we found that on 4d Rh(111) and Pd(111) surfaces, three-fold hollow sites are energetically favorable compared with singly coordinated top sites, with magnitudes of 0.57 and 0.87 eV, respectively. While for 5d Pt(111), NO adsorption in the hollow sites is still energetically more favorable than the top sites, however the difference decreases. For NO/Ir(111), the site preference is reversed, and the top sites become energetically favorable by 0.10 eV more than the hollow sites. On the other hand, we note that although fcc and hcp site adsorption are both three-fold coordinated, the difference lies in the third metal layer underneath, and the corresponding energetics change is modest. From Table 2, it can be found that on Pd(111) and Ir(111),

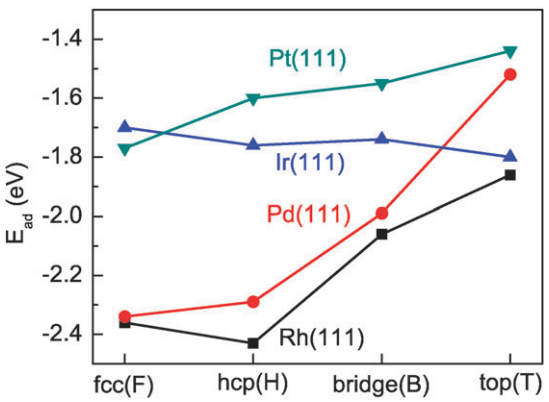

Fig. 3 The calculated adsorption energies for NO in various sites at 0.25 ML.

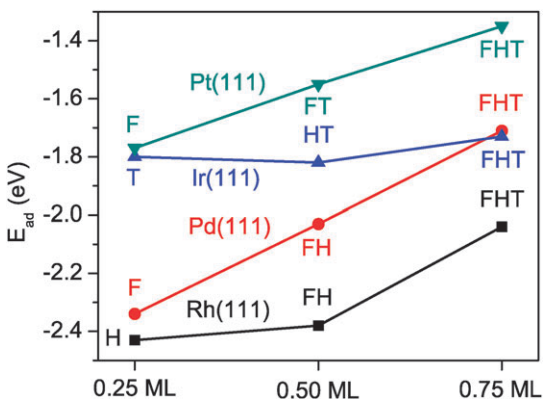

Fig. 4 The average adsorption energy for NO adsorption in the energetically most favorable sites at coverages of 0.25, 0.50 and 0.75 ML.

Table 2 Calculated average adsorption energy (in eV) for NO adsorption in various sites and different coverages. T(p) and T(t) represents the perpendicular and tilted top site NO, respectively. For NO adsorption at 0.50 ML, $p(2 \times 2)$ unit cells were employed except FH^c using the $c(4\times2)$ unit cell. The favorable configurations at a given coverage are indicated by bold font

	0.25 ML					0.50 ML				0.75 ML
	F	H	B	T(p)	T(t)	FH	FT	HT	FH^c	FHT
Rh	−2.36	**−2.43**	−2.06	−1.86	—	−2.26	−1.99	−2.05	**−2.38**	**−2.04**
Pd	**−2.34**	−2.29	−1.99	−1.18	−1.52	−1.92	−1.86	−1.83	**−2.03**	**−1.71**
Ir	−1.70	−1.76	−1.74	**−1.80**	—	−1.80	−1.80	**−1.82**	−1.80	**−1.73**
Pt	**−1.77**	−1.60	−1.55	−0.86	−1.44	−1.38	**−1.55**	−1.49	−1.43	**−1.35**

Published on 26 January 2010 on http://pubs.rsc.org | doi:10.1039/B920857G
Downloaded by Dalian Institute of Chemical Physics, CAS on 02/05/2013 07:43:48.

calculated adsorption energies for the fcc hollow-site NO is 0.05 and 0.06 eV lower than the hcp site NO, while on Rh(111) and Pt(111), the hcp site NO is more favorable than the fcc site NO by 0.07 and 0.17 eV, respectively.

The dependence of the site preference and the energetic difference between various sites on TMs reflects the local minima of the potential energy surface for NO adsorption. As shown in Fig. 3, the difference between various sites is modest for Ir(111), which indicates a flat potential energy surface for NO adsorption. While it becomes slightly corrugated for NO/Pt(111). It becomes rough however for 4d TMs, and the maximum differences between the different sites are 0.57 and 0.82 eV for Rh(111) and Pd(111), respectively. This is understandable since 4d TMs are more active than 5d TMs in the same column. The higher activity of 4d TMs than 5d TMs also rationalizes the stronger bonding strength of 4d TMs. For NO adsorption at the top sites, we note that adsorbed NO is perpendicular to Rh(111) and Ir(111) surfaces. Whereas on Pd(111) and Pt(111), NO prefers the tilted configuration, and the energy gains *via* tilting are 0.34 and 0.58 eV, respectively. These results are essential to understanding NO adsorption at high coverage, and the underlying mechanism will be discussed in detail during the following electronic analysis.

At higher coverage, 0.50 ML, the most favorable configurations are $c(4 \times 2)$-2NO(FH) for Rh(111) and Pd(111), $p(2 \times 2)$-2NO(HT) for Ir(111) with average adsorption energies of −2.38, −2.03 and −1.82, respectively. While on Pt(111), the most favorable structure is $p(2 \times 2)$-2NO(FT) with an energy of −1.55 eV. The formation of these structures can be explained using the corresponding potential energy surface at 0.25 ML as discussed above. For Rh(111) and Pd(111), which have a highly corrugated potential energy surface and strong site preference for NO in hollow sites, additional NO prefers to populate empty hollow sites at the cost of sharing surface metal atoms. This leads to the formation of $c(4 \times 2)$-2NO(FH) structure by minimizing bond competition (surface TM atoms coordinated by more than one NO), instead of the $p(2 \times 2)$-2NO(FH) structure (see the discussion in Section 4), as indicated in Figs. 2(a) and (b). For a flat potential energy surface such as Ir(111) and even Pt(111), the bond competition and electrostatic repulsion become important. Correspondingly, $p(2 \times 2)$-2NO(HT) for Ir(111) and $p(2 \times 2)$-2NO(FT) for Pt(111) are preferential since there is no site competition. At a coverage of 0.75 ML, we calculated several configurations, and found the fcc + hcp + top (FHT) structure has the lowest energy for all TMs, as plotted in Fig. 2(d). This configuration is energetically favorable, and the calculated average adsorption energies are −2.04, −1.71, −1.73, −1.35 eV for Rh, Pd, Ir and Pt, respectively.

In Fig. 4, the calculated adsorption energies in the energetically most favorable sites at a given coverage are plotted. For NO adsorption on Rh, Pd and Pt, the adsorption energies increase with the coverage, which indicates a lateral NO–NO repulsion between adsorbates. While for Ir, the variation of adsorption energies at different coverages is small, and this is in-line with the flat potential energy surface of NO/Ir(111) discussed at 0.25 ML.

Calculated adsorption energies and site preferences are in good agreement with previous calculations.[12,14,25–28,30–36] Moreover, these results explain the experimental findings well. For NO/Ir(111), the top-site preference was found experimentally for coverage less than 0.25 ML, as found in the present calculations. At higher coverage, NO adsorption at fcc hollow sites was suggested,[15] and in addition, no ordered structure has been reported yet. According to our work, the absence of the ordered NO structure on Ir(111) may come from the weak lateral interaction between adsorbed NO molecules and a flat potential energy surface. At coverages higher than 0.25 ML, occupancy of both hcp and fcc sites is possible due to the small adsorption energy difference, *i.e.*, −1.82 eV (FT) and −1.80 eV (HT).

For NO/Rh(111), the structures formed remains elusive. For example, experimental studies indicated a preference for fcc sites at low coverage, and occupancy of the top sites with increasing coverage, and finally the hcp hollow sites were occupied at higher coverage.[6–9,25] However, TPD experiments for NO-saturated surfaces found that top-site NO desorbed first, and both fcc and hcp NO desorbed at about same temperatures, which indicates that the structures at moderate NO coverage would be fcc + hcp,[8] instead of the fcc + top structure mentioned above. Our calculations, which are consistent with previous calculations,[12,14,27,28] supports the model proposed from TPD measurements.

3.3 Geometric parameters

The geometric parameters defined in Fig. 1 are summarized in Table 3 for the energetically most favorable structure at a given coverage. For comparison, available experimental data are also included. We found that NO adsorption induces a slight expansion of the topmost interlayer spacing (positive Δd_{12}), which increases with coverage. The surface buckling, Δ_z, is significant for Ir(111), with a magnitude of 0.25 Å, but modest for Rh(111), Pd(111) and Pt(111). These results are in good agreement with previous DFT calculations[27,36] and available experiments.[6,10,16,17,21]

 This journal is © the Owner Societies 2010

View Article Online

Table 3 Structural parameters for NO adsorption on the TM surfaces considered, as defined in Fig. 1: bond length of NO, d_{N-O}; bond length between N and metal atoms underneath, d_{N-TM}; height of N and O to the TM surfaces, h_{N-TM} and h_{O-TM}; angle between the normal to the surface and the NO molecule, α; interlayer spacing relaxations, Δd_{ij}, and buckling parameter, Δ_z. The experimental results for Rh (ref. 6), Pd (ref. 10) and Pt (ref. 21) are given in parentheses for comparison

Θ_{NO} (ML)	Conf.	Sites	d_{N-O} (Å)	d_{N-TM} (Å)	h_{N-TM} (Å)	h_{O-TM} (Å)	α (Degree)	Δd_{12} (%)	Δd_{23} (%)	Δ_z (Å)
Rh										
0.25	H	hcp	1.22	2.04	1.32	2.53	1.1	+1.25	−2.03	0.11
0.50	FH	fcc	1.21	2.07	1.40	2.60	3.3	+3.08	−1.62	0.12
		hcp	1.21	2.06	1.38	2.59	3.9			
0.75	FHT	fcc	1.22	2.07	1.30	2.52	0.3	+3.94	−1.62	0.18
			(1.15)	(2.03)	(1.3)	(2.45)	(0.0)	(+4.01)	(−1.28)	(0.00)
		top	1.17	1.79	1.92	3.09	4.9	—	—	—
			(1.13)	(1.76)	(1.76)	(2.89)	(0.0)	—	—	—
		hcp	1.22	2.01	1.30	2.52	0.4	—	—	—
			(1.18)	(2.03)	(1.3)	(2.47)	(0.0)	—		—
Pd										
0.25	F	fcc	1.21	2.04	1.26	2.47	0.0	+1.74	+0.14	0.13
0.50	FH	fcc	1.21	2.07	1.31	2.51	5.9	+2.57	+0.44	0.14
			(1.22)	(2.01)	(1.24)	(2.45)	(8)	(+2.41)	(+1.07)	(0.16)
		hcp	1.20	2.08	1.34	2.54	5.3	—	—	—
			(1.23)	(2.02)	(1.27)	(2.49)	(8)	—	—	—
0.75	FHT	fcc	1.21	2.08	1.27	2.48	0.7	+2.91	+0.57	0.15
			(1.27)	(2.02)	(1.20)	(2.46)	(7)	(+2.85)	(+0.63)	(0.11)
		top	1.18	1.93	2.02	2.85	42.6	—	—	—
			(1.16)	(1.86)	(1.94)	(2.73)	(47)	—	—	—
		hcp	1.20	2.09	1.30	2.51	1.3	—	—	—
			(1.21)	(2.07)	(1.29)	(2.50)	(4)	—	—	—
Ir										
0.25	T	top	1.18	1.78	2.00	3.18	1.1	+0.36	−1.54	0.30
0.50	HT	top	1.17	1.78	2.01	3.18	0.9	+2.21	−1.75	0.20
		hcp	1.23	2.10	1.27	2.51	0.1	—	—	—
0.75	FHT	fcc	1.23	2.10	1.31	2.54	0.1	+3.33	−1.52	0.25
		top	1.17	1.79	1.98	3.14	1.1	—	—	—
		hcp	1.22	2.11	1.33	2.56	0.1	—	—	—
Pt										
0.25	F	fcc	1.21	2.10	1.31	2.52	0.0	+2.11	−0.05	0.18
			(1.19)	(2.07)	(1.31)	(2.50)	(0.00)	(+1.77)	(−0.44)	(0.08)
0.50	FT	fcc	1.22	2.08	1.21	2.43	0.8	+2.94	+0.24	0.18
			(1.21)	(2.01)	(1.22)	(2.43)	(2.0)	(+2.93)	(−0.18)	(0.08)
		top	1.18	1.96	2.09	2.85	49.3	—	—	—
			(1.14)	(1.94)	(1.99)	(2.73)	(49.3)	—	—	—
0.75	FHT	fcc	1.22	2.09	1.26	2.48	1.3	+3.64	+0.48	0.17
			(1.17)	(2.09)	(1.28)	(2.45)	(0.40)	(+2.85)	(+0.65)	(0.10)
		top	1.18	1.96	2.06	2.89	45.3	—	—	—
			(1.12)	(1.99)	(2.05)	(2.76)	(50.5)	—	—	—
		hcp	1.21	2.10	1.33	2.54	1.3	—	—	—
			(1.15)	(2.01)	(1.34)	(2.53)	(0.10)	—	—	—

Downloaded by Dalian Institute of Chemical Physics, CAS on 02/05/2013 07:43:48.
Published on 26 January 2010 on http://pubs.rsc.org | doi:10.1039/B920857G

We found that the change of the bond length of NO (d_{N-O}) upon adsorption in the top sites is negligible. However, d_{N-O} increases from 1.17 Å in the gas phase to about 1.20–1.23 Å for NO in the hollow sites. This indicates a pronounced weakening of the N–O bond at the hollow sites, as corroborated by significant red-shift of N–O stretching in the range of 200 to 300 cm^{-1} for hollow-site NO.[8,9,15,20,27] The red-shift and larger N–O bond length for hollow-site NO comes from the enhanced electron back-donation from metal d-bands to NO $2\pi^*$ orbitals, as discussed in Section 3.4 below. In this context, we note that the large red-shift and elongation of N–O bond length, which are site sensitive, do not necessarily lead to the strong bonding between adsorbed NO and the substrates underneath. This can be seen for NO/Ir(111) at 0.25 ML, in which top-site NO is energetically favorable, but the corresponding N–O bond length is shorter than hollow-site NO. Concerning the N–TM bond length (d_{N-TM}), it is noticeably larger for NO in the hollow site (varies from 2.01–2.10 Å) than that of the top-site NO (varies from 1.78–1.96 Å) due to the different coordination numbers.

For all calculated structures, NO molecules in the hollow sites are perpendicular to the surface at low coverage, and become tilted with angle of around 6° with respect to normal direction at high coverage due to the lateral NO–NO repulsion. The tilting found here was indeed found during recent experiments for NO adsorption on Pd(111) at finite temperature.[10] We note however that the measured tilting angle (8°) was slightly larger than the calculated one at absolute zero temperature. To quantify the effect of temperature, we performed *ab initio* molecular dynamics at the corresponding experimental temperature, and found that the tilting angle indeed increase by about 2°, which agrees well with experimental results.[65] Top-site NO prefers the upright configuration on Rh(111) and Ir(111). In contrast, top-site NO on Pd(111) and Pt(111) are tilted significantly from the normal direction (α, as defined in Fig. 1) by about 40° to 50°. Calculated α values are in good

Downloaded by Dalian Institute of Chemical Physics, CAS on 02/05/2013 07:43:48.
Published on 26 January 2010 on http://pubs.rsc.org | doi:10.1039/B920857G

agreement with available experimental measurements,[10,16,17,21] and previous calculations.[12,14,26,31,33,36] We note that the tilted top NO was also found for NO adsorption on Ag(111) and Au(111) surfaces[28] and the underlying mechanism has been discussed in several papers.[28,35,36] A general principle underlining this will be given below.

3.4 Projected density of states

Insights into the interaction between NO and TM surfaces can be obtained from the projected density of states (PDOS). To visualize the hybridization between TM bands and NO molecular orbitals efficiently, generic NO σ- and π-orbitals were defined by sum of the corresponding N and O $p_{x,y}$ and p_z's PDOS,[36]

$$\pi = N_{p_x} + N_{p_y} + O_{p_x} + O_{p_y}, \quad (2)$$

$$\sigma = N_s + N_{p_z} + O_s + O_{p_z}. \quad (3)$$

The calculated π- and σ-orbitals for NO and the PDOS of surface metal atoms coordinated with NO are plotted in Fig. 5 for fcc and top (perpendicular and tilted) site adsorption at 0.25 ML. PDOS can be divided into two energy

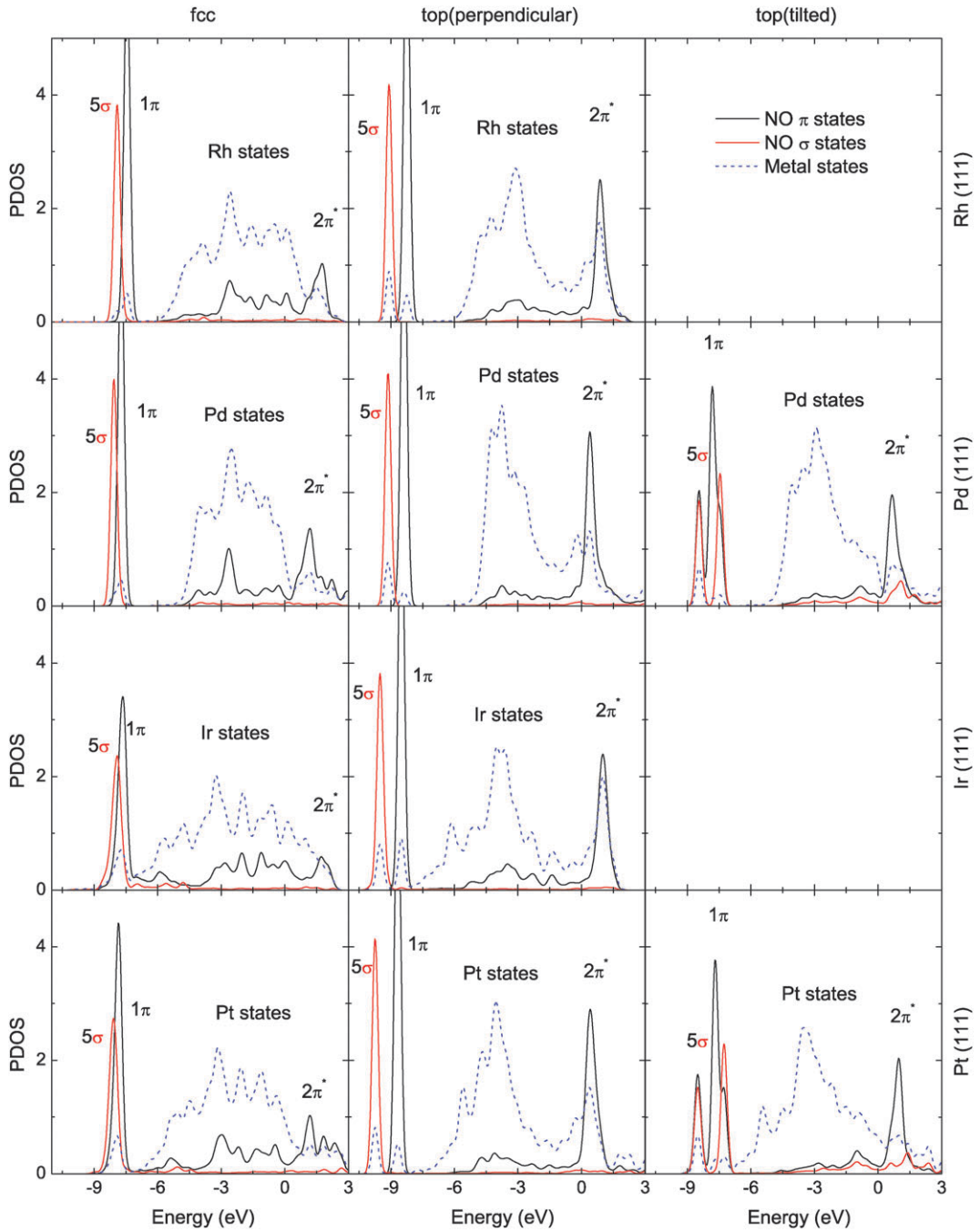

Fig. 5 Projected density of states for NO adsorption (0.25 ML) on the TM surfaces considered. NO π- and σ-orbitals are calculated according the formula given in the main text. The zero references are the Fermi level.

 This journal is © the Owner Societies 2010

Downloaded by Dalian Institute of Chemical Physics, CAS on 02/05/2013 07:43:48.
Published on 26 January 2010 on http://pubs.rsc.org | doi:10.1039/B920857G

windows: [−6 eV, 0 eV] for the hybridization between NO 2π* orbitals and the TM's d-band, and [−10 eV, −7 eV] for the hybridization between 1π, 5σ and the TM's d-band. For the deep-lying orbitals, the 1π orbital is slightly higher than the 5σ orbital, and the relative difference is site and configuration dependent. In this context, we note that the order of 1π and 5σ orbital here is different from NO in the gas phase.[36]

For NO adsorption at hollow sites, the geometry is favorable for the hybridization between NO π-orbitals and TM $d_{xz,yz}$ orbitals, and this in turn facilitates charge transfer from TMs to NO π-orbitals. In contrast, for top-site NO (perpendicular), though both 1π and 5σ orbitals are lowered, it is more pronounced for 5σ orbitals because the specific configuration is favorable for NO 5σ and TM d_{z^2} hybridization. Correspondingly, the donation from NO 5σ to TM d_{z^2} is significant. For tilted top NO, the configuration promotes the interaction of NO π-orbitals with TM $d_{xz,yz}$ orbitals and related back-donation processes.

To quantify the amount of charge transfer induced by adsorption, we integrated NO's σ and π PDOS 'till the Fermi level. In the gas phase, NO has eleven electrons (*e*) in the occupied orbitals, namely, six in σ-orbitals and five in π-orbitals, and the highest occupied π-orbital is half occupied. These were used to normalize the PDOS integration for adsorbate–substrate systems, and the difference with respect to NO in the gas phase is given in Table 4. We found that upon adsorption, irrespective of the adsorption sites and TM surfaces, the charge increases typically by more than half an electron for NO π-orbitals, while decreasing by about 0.40 electrons for NO σ-orbitals. The overall charge transfer (Δπ + Δσ) therefore results in a net electronic accumulation on adsorbed NO.

Table 4 The change of electron population in NO σ- and π-orbitals with respect to NO in the gas phase as well as the net charge gain (Δπ + Δσ) due to adsorption on TM surfaces at 0.25 ML. T(p) and T(t) represent the perpendicular and tilted top-site NO, respectively

	Site	Δπ	Δσ	Δπ + Δσ
Rh	B	0.62	−0.23	0.39
	F	0.67	−0.30	0.36
	H	0.67	−0.31	0.35
	T	0.50	−0.10	0.40
Pd	B	0.53	−0.19	0.35
	F	0.62	−0.26	0.37
	H	0.59	−0.26	0.34
	T(p)	0.36	−0.07	0.29
	T(t)	0.56	−0.23	0.33
Ir	B	0.65	−0.27	0.38
	F	0.71	−0.37	0.34
	H	0.71	−0.36	0.35
	T	0.59	−0.13	0.46
Pt	B	0.59	−0.23	0.36
	F	0.68	−0.32	0.36
	H	0.65	−0.30	0.35
	T(p)	0.44	−0.10	0.34
	T(t)	0.56	−0.23	0.33

The above analyses show that the interaction between NO and TM surfaces follows a donation and back-donation process in general. This mechanism was discussed for NO adsorption on Pt(111),[35,36] and extended to more TMs in present work. In the literature, the interaction between CO and Pt(111) TMs was found to be similar.[66–76]

The electronegativity of both O and N atoms are significant larger than that of the TMs considered, *e.g.*, Pauling electronegativities are 3.44 and 3.04 for O and N, and about 2.2 for Rh, Pd, Ir and Pt, respectively.[77] Hence, a charge transfer from substrates to adsorbed NO upon NO adsorption is expected. This is in-line with the above findings. Despite the net charge gain for adsorbed NO molecules, the spatial charge redistribution and change of work function with respect to the bare surface are site dependent, which will be discussed below.

3.5 Work function changes

It is well know that the adsorption of adatoms on surfaces induces a change of work function with respect to bare surfaces ($\Delta\Phi = \Phi^{NO/TM(111)} - \Phi^{TM(111)}$), whose sign and magnitude reflect the direction of charge transfer and electron redistribution. Calculated $\Delta\Phi$ values are summarized in Table 5. In addition, adsorption-induced dipole moments, μ, defined by the Helmholtz equation,[78,79] $\mu = 1/12\pi \times A\Delta\Phi/\theta$, where A is the area per (1 × 1) surface unit cell in Å^2. Positive μ indicates an inward-pointing surface dipole moment (*i.e.*, the negative end is outside of the surface), while negative

Table 5 Adsorption-induced change of surface work function with respect to bare surfaces ($\Delta\Phi$ in eV) and dipole moment (μ in Debye). T(p) and T(t) represent the perpendicular and tilted top-site NO, respectively. For NO adsorption at 0.50 ML, $p(2 \times 2)$ unit cells were employed except FH[c], where $c(4 \times 2)$ was used instead. The calculated surface work functions for the clean surfaces are 5.13, 5.27, 5.45 and 5.73 eV for Rh(111), Pd(111), Ir(111) and Pt(111), respectively. Bold fonts corresponds to the results for the energetically most favorable structure at a given coverage

	0.25 ML					0.50 ML				0.75 ML
	F	H	B	T(p)	T(t)	FH	FT	HT	FH[c]	FHT
Rh										
$\Delta\Phi$	0.74	**0.78**	0.57	−0.36	—	1.10	0.28	0.27	**1.20**	**0.69**
μ	0.50	**0.53**	0.39	−0.24	—	0.37	0.09	0.09	**0.41**	**0.16**
Pd										
$\Delta\Phi$	**0.45**	0.39	0.10	−0.68	−0.27	0.49	0.08	−0.04	**0.50**	**0.26**
μ	**0.32**	0.28	0.07	−0.49	−0.19	0.18	0.03	−0.01	**0.18**	**0.06**
Ir										
$\Delta\Phi$	0.70	0.65	0.36	**−0.65**	—	1.04	0.08	**0.06**	1.04	**0.52**
μ	0.48	0.45	0.25	**−0.45**	—	0.36	0.03	**0.02**	0.36	**0.12**
Pt										
$\Delta\Phi$	**0.34**	0.18	−0.14	−1.22	−0.41	0.30	**−0.05**	−0.13	0.31	**0.14**
μ	**0.25**	0.13	−0.10	−0.90	−0.30	0.11	**−0.02**	−0.05	0.11	**0.03**

Downloaded by Dalian Institute of Chemical Physics, CAS on 02/05/2013 07:43:48.
Published on 26 January 2010 on http://pubs.rsc.org | doi:10.1039/B920857G

μ indicates an outward-pointing surface dipole moment (to the vacuum).

The above PDOS analysis at 0.25 ML indicates a net charge transfer from substrates to the adsorbed NO, irrespective of the adsorption sites and the TM surfaces studied. Hence, an increase in work function (positive $\Delta\Phi$) would be expected upon NO adsorption. This is indeed found for hollow-site NO, and a positive $\Delta\Phi$ means an inward pointing surface dipole moment induced by adsorption. For top-site NO, however, the surface work function decreases upon adsorption, and correspondingly, the direction of the dipole moment points outward to the vacuum. The site dependence of the surface dipole moment induced by adsorption plays an important role in the lateral (electrostatic) interaction between adsorbates. The balance between lateral interaction and energetics at different sites, which are element dependent, determines the structures formed at different coverages.

For FT and HT structures at 0.50 ML, the calculated absolute values of $\Delta\Phi$ are small. This is because hollow-site NO and top-site NO have the opposite surface dipole moments. While for the FH structure, the calculated $|\Delta\Phi|$ remains significant because the direction of the surface dipole moment induced by both fcc and hcp NO are same. As a consequence, the electrostatic repulsion between fcc and hcp NO is developed. This results in so-called depolarization, as seen clearly from the decrease of the surface dipole moment μ, for instance 0.37 (Rh), 0.18 (Pd), 0.36 (Ir) and 0.11 (Pt) Debye, compared to 0.50, 0.32, 0.48 and 0.25 Debye for fcc hollow NO at 0.25 ML, respectively. For NO adsorption at 0.75 ML, a common structure (FHT) forms on the four TMs considered. This structure can be described as a superposition of the FH (0.50 ML) and T (0.25 ML) structures. Since top-site NO has the opposite dipole moment with respect to hollow-site NO, the calculated $\Delta\Phi$ is smaller than the FH structure at 0.50 ML, correspondingly.

The change of the work function $\Delta\Phi$ as function of the coverage is plotted in Fig. 6 for the energetically most favorable structures at a given coverage. Rather different behavior on the various TMs can be clearly seen. For NO/Ir(111), the work function decreases at low coverage of 0.25 ML because

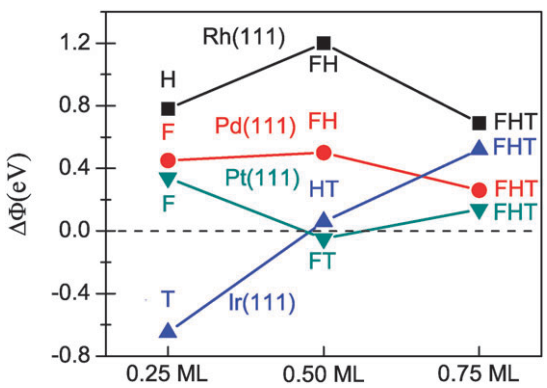

Fig. 6 The change of work function (with respect to bare surfaces) induced by adsorbed NO. At a given coverage only the results for the energetically most favorable structures are given.

of the NO adsorption in the top sites. It becomes positive however and increases monotonically with coverage due to the gradual occupation of hollow-site NO. In contrast, for NO adsorption on Rh and Pd, the work function increases at 0.25 and 0.50 ML due to NO adsorption at hollow sites, and it decreases at 0.75 ML due to the occupation of the top sites by NO. For Pt(111), the work function increases at 0.25 ML, as found for Rh and Pd. It decreases at 0.50 ML because of the presence of top-site NO, and it increases again at 0.75 ML due to the presence of the additional hollow-site NO. These analyses show clearly that the work function changes induced by NO at different coverages are dominated by the occupation of NO at various sites, which are TM dependent. Calculated results are in good agreement with available experimental data. For instance, for NO/Pt(111), the measured surface work function increases by about 0.14 eV at 0.17 ML, but decreases to −0.16 eV at 0.52 ML.[5] For NO on Rh, Pd and Ir(111), to best of our knowledge, there is no systematic measurement of the surface work function yet for comparison.

3.6 Electron density differences

To shed light on the work function change, we analyzed the charge transfer induced by NO adsorption, employing the electron density differences $\rho^{\Delta}(\mathbf{r})$. $\rho^{\Delta}(\mathbf{r})$ obtained using

$$\rho^{\Delta}(\mathbf{r}) = \rho^{\mathrm{NO/TM(111)}}(\mathbf{r}) - \rho^{\mathrm{TM(111)}}(\mathbf{r}) - \rho^{\mathrm{NO}}(\mathbf{r}). \qquad (4)$$

We also analyzed the average planar electron density differences in the xy plane and along the normal direction (z-axis), $\bar{\rho}^{\Delta}(z)$. Our results for NO in the fcc, top (perpendicular), and top (tilted) sites (0.25 ML) are shown in Fig. 7.

It can be seen that the charge density redistributions are located mainly in the topmost metal layer and adsorbed NO, while slight perturbations are observed in the second *meta* layers. These charge redistributions originate from charge transfer and polarizations, which are in turn site-dependent due to the nature of the metal d-bands involved and hybridization with adsorbed NO molecules. For NO adsorption in the hollow sites, the variation of the TM's $d_{xz,yz}$ bands is notable, while variation of the TM's d_{z^2} bands is notable for NO adsorption in the top sites. Nevertheless, both $d_{xz,yz}$ and d_{z^2} show a pronounced depletion, which is the source of the back-donation from substrates to adsorbates. For NO, a depletion of the O and N p_z–(5σ–) states with a polarization around nitrogen was found, which can be attributed to the source of electron donation from NO to TM substrates. The electron accumulation is mainly distributed in the N and O $p_{x,y}$–($2\pi^*$–) states and in the bonding region between adsorbate and substrate.

The opposite signs of $\Delta\Phi$ for NO in the hollow and top sites can be understood from the planar averaged electron density differences $\bar{\rho}^{\Delta}(z)$, which are shown in Fig. 7. To illustrate this, the mass center of the accumulated charge ($\bar{\rho}^{\Delta}_{+}(z)$, positive part of $\bar{\rho}^{\Delta}(z)$) and depleted charge ($\bar{\rho}^{\Delta}_{-}(z)$, negative part of $\bar{\rho}^{\Delta}(z)$), *i.e.*, z_{ρ}^{+} and z_{ρ}^{-}, are defined:

$$z_{\rho}^{+} = \frac{1}{q}\int_{0}^{c/2} \bar{\rho}^{\Delta}_{+}(z) z \mathrm{d}z, \text{ and } z_{\rho}^{-} = -\frac{1}{q}\int_{0}^{c/2} \bar{\rho}^{\Delta}_{-}(z) z \mathrm{d}z,$$

 This journal is © the Owner Societies 2010

Downloaded by Dalian Institute of Chemical Physics, CAS on 02/05/2013 07:43:48.
Published on 26 January 2010 on http://pubs.rsc.org | doi:10.1039/B920857G

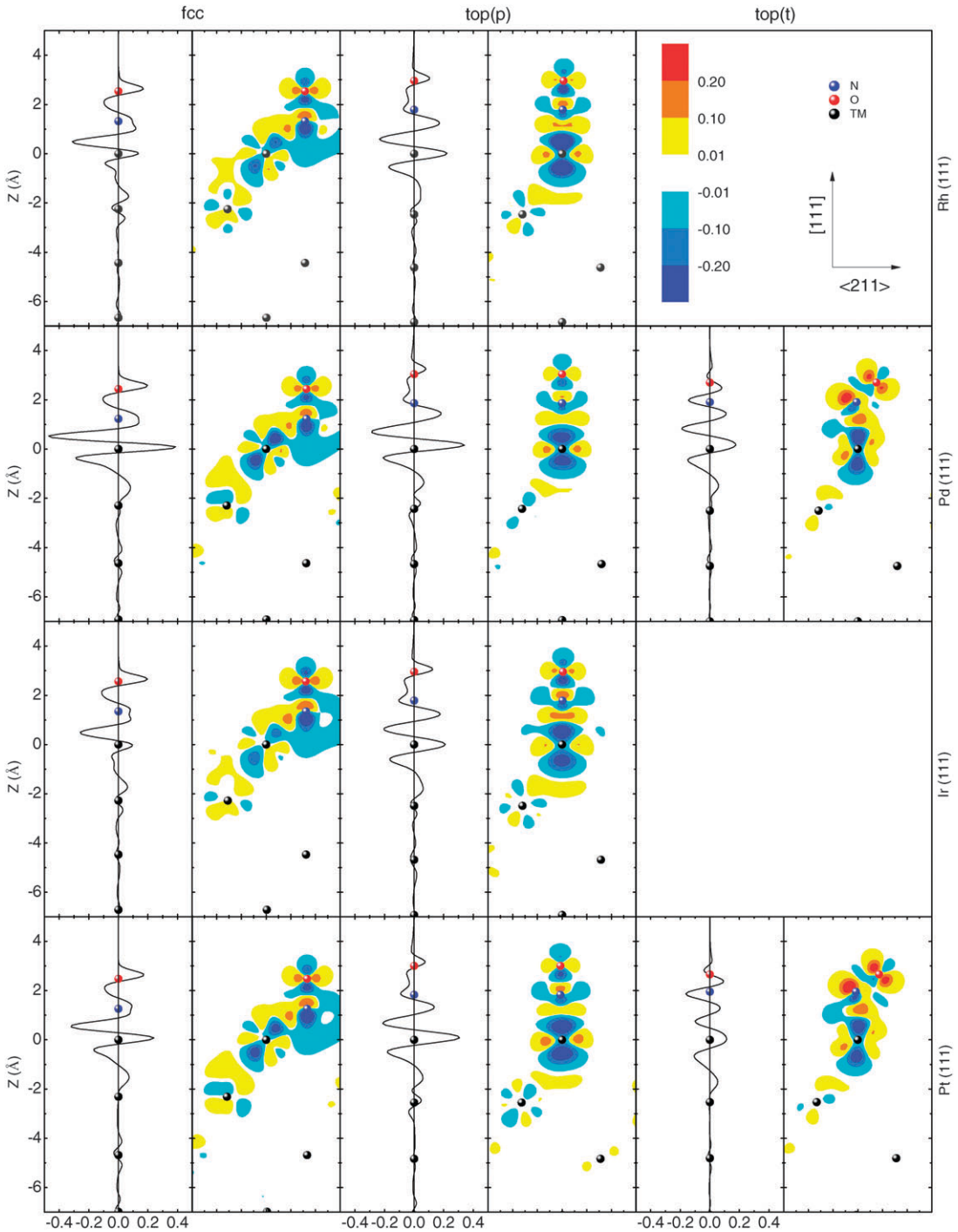

Fig. 7 Calculated average electron density differences $\bar{\rho}^{\Delta}(z)$ (left column) and $\rho^{\Delta}(r)$ (right column) for NO adsorbed in the fcc, perpendicular top (top(p)) and tilted top (top(t)) sites (0.25 ML) along the (211) planes through N and O atoms. Cyan to blue (yellow to red) indicates the depletion (accumulation) of the electron density. N, O and Pt atoms are indicated by blue, red and dark gray spheres respectively. The unit is e Å^{-3} for $\rho^{\Delta}(\mathbf{r})$ and e Å^{-1} for $\bar{\rho}^{\Delta}(z)$.

where the integral range is a complete dimension of the supercell, and q is the amount of the overall charge redistributions, and calculated by

$$q = q^{+} = -q^{-} = \int_0^2 \bar{\rho}_{+}^{\Delta}(z)\mathrm{d}z = -\int_0^2 \bar{\rho}_{-}^{\Delta}(z)\mathrm{d}z.$$

From these equations, the dipole moment induced by adsorption can be obtained by

$$\mu = q(z_{\rho}^{+} - z_{\rho}^{-}) = \int_0^2 \bar{\rho}^{\Delta}(\mathbf{z})z\mathrm{d}z, \qquad (5)$$

The results for μ, z_{ρ}^{+} and z_{ρ}^{-} are summarized in Table 6.

Downloaded by Dalian Institute of Chemical Physics, CAS on 02/05/2013 07:43:48.
Published on 26 January 2010 on http://pubs.rsc.org | doi:10.1039/B920857G

Table 6 Adsorption-induced surface dipole moment μ calculated by integration of the planar average electron density difference *via* eqn (5) at 0.25 ML. z_ρ^+ and z_ρ^- represent the mass center of accumulated and depleted charge with respect to the mass center of surface metal atoms

Metal	Structure	μ/Debye	z_ρ^+/Å	z_ρ^-/Å
Rh	F	0.49	0.50	0.05
	T	−0.03	0.23	0.26
Pd	F	0.53	0.22	0.09
	T(p)	−0.24	0.15	0.32
	T(t)	−0.10	0.17	0.27
Ir	F	0.44	0.61	0.18
	T	−0.22	0.17	0.35
Pt	F	0.35	0.55	0.27
	T(p)	−0.51	0.32	0.71
	T(t)	−0.10	0.53	0.65

Compared with μ calculated from the Helmholtz equation (see Table 5), we found that both approaches yield the same trends. The opposite dipole moment of hollow and top sites adsorption can be clearly seen from the relative positions of z_ρ^+ and z_ρ^+. Namely, z_ρ^+ is higher than z_ρ^- for hollow-site NO adsorption, while it is opposite for top-site NO adsorption. The inversion of z_ρ^+ and z_ρ^- from hollow-site NO adsorption to top-site NO adsorption mainly comes from the fact that for the latter one, there is a pronounced enhancement of charge accumulation between NO and surface metal atoms underneath about 1.5 Å.

The driving force for the outward dipole moment induced by the top-site NO comes from specific configuration and related hybridization between NO and TMs, despite overall charge transfer from substrates to adsorbed NO. In this context, we note that outward dipole moments and decrease of the work function induced by electronegative species upon adsorption was found in literature also for atomic nitrogen adsorption on W(100) surfaces by Michaelides *et al.*[80] In that case, the nitrogen atom adsorbed at four-fold hollow sites, and it is the reduction in the surface overspill electron density into the vacuum that leads to the decrease of the work function.

4. Discussion

The interesting and yet complicated results for NO adsorption on TM surfaces shown above come mainly from the characteristic potential energy surface for NO adsorption on different TM surfaces at low coverage. Understanding of underlying mechanism was therefore fundamentally important, and discussed in this section. First, we note that the large adsorption energy and extensive hybridization between NO and TM surfaces are characteristic of chemisorption. The interaction follows a donation–back-donation process, namely, charge donation from NO 5σ orbitals to TM d-bands, whilst back-donation from TM d-bands to the NO 2π*-orbitals occurs. As shown in Table 4, irrespective of adsorption site and TM, the back-donation is always larger than that of the donation, which results in an overall net charge transfer from substrates to adsorbed NO. On the other hand, we note that the amount of donation and back-donation is site dependent, and both of them increase with the coordination number. This is understandable since multiple coordination adsorption would facilitate the charge transferring and be

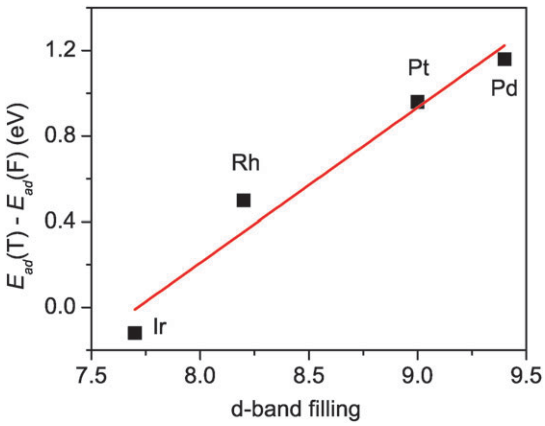

Fig. 8 The adsorption energy difference between fcc and top (perpendicular) site NO at 0.25 ML with respect to d-band filling.

energetically preferred. As a consequence, the site preference for NO adsorption in the high-coordinate sites as well as the energetic difference between various sites with distinct coordinations would be determined by the extent of donation and back-donation between NO and substrates, which is element dependent. Since TM d-bands are significantly involved in both the donation and back-donation processes, determining how many d-electrons are available (namely filling of d-bands) for electron transfer is therefore essential.

In this context, we note that the TMs considered here do have very different d-band fillings, and calculated values are 7.7, 8.2, 9.0 and 9.4 *e* for Ir, Rh, Pt and Pd(111) surfaces, respectively. To illustrate the role of TM d-band filling, we calculated the NO adsorption energy difference between top (perpendicular) and hollow sites, and its dependence on the d-band filling of different TMs, and plotted the results in Fig. 8. A linear correlation between the adsorption energy difference and the d-band filling can be clearly seen. For Pd(111) with the largest d-band filling, the energy difference is significantly large with a value of 1.16 eV, namely the three-coordinate hollow sites are highly favorable. While for Pt(111) with a smaller d-band filling, the difference decreases to the value of 0.91 eV. With an decrease in d-band filling further to Rh, the energy difference decreases continuously, and actually the top site even becomes favorable for Ir with the least d-band filling. This result shows unambiguously that the preference of high coordination sites for NO adsorption on TM surfaces is determined by d-band filling, as suggested above.

The effect of TM d-band filling further explains the fact that the tilting of top-site NO occurs on Pd and Pt with an energy gain of 0.34 eV and 0.58 eV, instead of Rh and Ir. A simple geometric consequence of the tilting of top-site NO is an increase of effective coordination, which would increase the extent of the donation and back-donation (see Table 4). For example, by tilting of perpendicular top-site NO, the amount of donated (σ) and back-donated (π) charge increases from 0.36 and −0.07 *e* to 0.56 and −0.23 *e* for Pd, and from 0.44 and −0.10 *e* to 0.56 and −0.23 *e* for Pt, respectively. This happens on Pd and Pt surfaces because of their higher d-band filling, compared to Rh and Ir. The stabilization gained from tilting of the top-site NO can be seen further from the upshift of

 This journal is © the Owner Societies 2010

View Article Online

Downloaded by Dalian Institute of Chemical Physics, CAS on 02/05/2013 07:43:48.
Published on 26 January 2010 on http://pubs.rsc.org | doi:10.1039/B920857G

hybridized states between NO 2π* and Pt/Pd d-bands (Fig. 5), which frees more energetically unfavorable antibonding states.

The effect of d-band filling on sites and geometries of molecule adsorption on platinum group surfaces highlighted here should apply in general to other similar systems, as indeed found in the literature. For instance, the tendency of tilting for NO in the top sites has been reported on Ag(111) and Au(111), in which the corresponding d-band is fully occupied.[28] In addition, the correlation between site preference and filling of the TM d-bands has been discussed for CO adsorption.[76]

5. Summary

In this work, we report a comprehensive first-principles study of the NO adsorption on close-packed transition metal Rh(111), Pd(111), Ir(111), and Pt(111) surfaces within a DFT framework as implemented in VASP. Valuable insights are obtained, and the fundamental principles for the interaction between NO and transition metal surfaces are illustrated. We find that the interaction between NO and TM(111) surfaces come from the donation and back-donation processes *via* the interplay between 5σ/2π*-orbitals and TM d-bands. Irrespective of the adsorption sites and TM, the amount of back-donated charge is larger than the donated charge, which leads to overall a net charge transfer from TM to adsorbed NO. Nevertheless, the change of work function induced by NO adsorption is site dependent, and the direction of surface dipole moments induced by hollow-site and top-site NO are opposite due to the different charge redistribution. On the other hand, the extent of donation and back-donation is correlated with coordination number. For TMs with large d-band filling such as Pd and Pt, three-coordinated hollow sites are energetically most favorable, and less favorable top-site NO prefers to tilt away from the normal direction. While for TMs with small d-band fillings such as Ir, top-site NO (perpendicular to the surfaces) is energetically most favorable. The present work indicates that the distinct potential energy surfaces and lateral interactions, which are TM dependent, are essential for NO adsorption on TM surfaces.

WXLI acknowledges financial support from the Natural Science Foundation of China (Contract Nos. 20503030,20733008,20873142), and the National Basic Research Program of China (2007CB815205). JLF Da Silva thanks the São Paulo Science Foundation (FAPESP).

References

1 B. E. Nieuwenhuys, *Adv. Catal.*, 1999, **44**, 259.
2 J. Kašpar, P. Fornasiero and N. Hickey, *Catal. Today*, 2003, **77**, 419.
3 J. C. L. Cornish and N. R. Avery, *Surf. Sci.*, 1990, **235**, 209.
4 C. Wögerbauer, M. Maciejewski and A. Baiker, *Appl. Catal., B*, 2001, **34**, 11.
5 M. Kiskinova, G. Pirug and H. P. Bonzel, *Surf. Sci.*, 1984, **136**, 285.
6 I. Zasada, M. A. Van Hove and G. A. Somorjai, *Surf. Sci.*, 1998, **418**, L89.
7 Y. J. Kim, S. Thevuthasan, G. S. Herman, C. H. F. Peden, S. A. Chambers, D. N. Belton and H. Permana, *Surf. Sci.*, 1996, **359**, 269.
8 I. Nakamura, Y. Kobayashi, H. Hamada and T. Fujitani, *Surf. Sci.*, 2006, **600**, 3235.
9 W. T. Wallace, Y. Cai, M. S. Chen and D. W. Goodman, *J. Phys. Chem. B*, 2006, **110**, 6245.
10 P. Kostelník, T. Šikola, P. Varga and M. Schmid, *J. Phys.: Condens. Matter*, 2009, **21**, 134005.
11 M. Bertolo and K. Jacobi, *Surf. Sci.*, 1990, **226**, 207.
12 R. T. Vang, J. G. Wang, J. Knudsen, J. Schnadt, E. Lægsgaard, I. Stensgaard and F. Besenbacher, *J. Phys. Chem. B*, 2005, **109**, 14262.
13 P. J. Chen and D. W. Goodman, *Surf. Sci.*, 1993, **297**, L93.
14 K. Højrup Hansen, Ž. Š. ljivančanin, B. Hammer, E. Lægsgaard, F. Besenbacher and I. Stensgaard, *Surf. Sci.*, 2002, **496**, 1.
15 T. Fujitani, I. Nakamura, Y. Kobayashi, A. Takahashi, M. Haneda and H. Hamada, *J. Phys. Chem. B*, 2005, **109**, 17603.
16 N. Materer, A. Barbieri, D. Gardin, U. Starke, J. D. Batteas, M. A. Van Hove and G. A. Somorjai, *Phys. Rev. B: Condens. Matter*, 1993, **48**, 2859.
17 N. Materer, A. Barbieri, D. Gardin, U. Starke, J. D. Batteas, M. A. Van Hove and G. A. Somorjai, *Surf. Sci.*, 1994, **303**, 319.
18 F. Esch, T. Greber, S. Kennou, A. Siokou, S. Ladas and R. Imbihl, *Catal. Lett.*, 1996, **38**, 165.
19 M. Matsumoto, N. Tatsumi, K. Fukutani, T. Okano, T. Yamada, K. Miyake, K. Hate and H. Shigekawa, *J. Vac. Sci. Technol., A*, 1999, **17**, 1577.
20 M. Matsumoto, K. Fukutani, T. Okano, K. Miyake, H. Shigekawa, H. Kato, H. Okuyama and M. Kawai, *Surf. Sci.*, 2000, **454–456**, 101.
21 M. Matsumoto, N. Tatsumi, K. Fukutani and T. Okano, *Surf. Sci.*, 2002, **513**, 485.
22 J. F. Zhu, M. Kinne, T. Fuhrmann, R. Denecke and H. P. SteinrÄijck, *Surf. Sci.*, 2003, **529**, 384.
23 P. Zhu, T. Shimada, H. Kondoh, I. Nakai, M. Nagasaka and T. Ohta, *Surf. Sci.*, 2004, **565**, 232.
24 W. A. Brown and D. A. King, *J. Phys. Chem. B*, 2000, **104**, 2578.
25 C. Popa, C. F. J. Flipse, A. P. J. Jansen, R. A. van Santen and P. Sautet, *Phys. Rev. B: Condens. Matter Mater. Phys.*, 2006, **73**, 245408.
26 M. Mavrikakis, J. Rempel, J. Greeley, L. B. Hansen and J. K. Nørskov, *J. Chem. Phys.*, 2002, **117**, 6737.
27 D. Loffreda, D. Simon and P. Sautet, *Chem. Phys. Lett.*, 1998, **291**, 15.
28 M. Gajdoš, J. Hafner and A. Eichler, *J. Phys.: Condens. Matter*, 2006, **18**, 13.
29 W. P. Krekelberg, J. Greeley and M. Mavrikakis, *J. Phys. Chem. B*, 2004, **108**, 987.
30 Q. Ge and D. A. King, *Chem. Phys. Lett.*, 1998, **285**, 15.
31 H. Aizawa, Y. Morikawa, S. Tsuneyuki, K. Fukutani and T. Ohno, *Surf. Sci.*, 2002, **514**, 394.
32 R. Burch, S. T. Daniells and P. Hu, *J. Chem. Phys.*, 2002, **117**, 2902.
33 D. C. Ford, Y. Xu and M. Mavrikakis, *Surf. Sci.*, 2005, **587**, 159.
34 H. Tang and B. L. Trout, *J. Phys. Chem. B*, 2005, **109**, 17630.
35 R. B. Getman and W. F. Schneider, *J. Phys. Chem. C*, 2007, **111**, 389.
36 Z.-H. Zeng, J. L. F. Da Silva, H.-Q. Deng and W.-X. Li, *Phys. Rev. B: Condens. Matter Mater. Phys.*, 2009, **79**, 205413.
37 P. E. Blöchl, *Phys. Rev. B: Condens. Matter*, 1994, **50**, 17953.
38 G. Kresse and D. Joubert, *Phys. Rev. B: Condens. Matter Mater. Phys.*, 1999, **59**, 1758.
39 P. Hohenberg and W. Kohn, *Phys. Rev.*, 1964, **136**, B864.
40 W. Kohn and L. J. Sham, *Phys. Rev.*, 1965, **140**, A1133.
41 J. P. Perdew, K. Burke and M. Ernzerhof, *Phys. Rev. Lett.*, 1996, **77**, 3865.
42 G. Kresse and J. Hafner, *Phys. Rev. B: Condens. Matter*, 1993, **48**, 13115.
43 G. Kresse and J. Furthmuller, *Phys. Rev. B: Condens. Matter*, 1996, **54**, 11169.
44 H. J. Monkhorst and J. D. Pack, *Phys. Rev. B: Solid State*, 1976, **13**, 5188.
45 C. Kittel, *Introduction to Solid State Physics*, John Wiley & Sons, New York, 7th edn, 1996.
46 M. Birgersson, C. O. Almbladh, M. Borg and J. N. Andersen, *Phys. Rev. B: Condens. Matter Mater. Phys.*, 2003, **67**, 045402.

View Article Online

47 J. L. F. Da Silva, C. Stampfl and M. Scheffler, *Surf. Sci.*, 2006, **600**, 703.
48 M. V. Ganduglia-Pirovano and M. Scheffler, *Phys. Rev. B: Condens. Matter Mater. Phys.*, 1999, **59**, 15533.
49 M. Todorova, K. Reuter and M. Scheffler, *J. Phys. Chem. B*, 2004, **108**, 14477.
50 S. Moré, A. P. Seitsonen, W. Berndt and A. M. Bradshaw, *Phys. Rev. B: Condens. Matter Mater. Phys.*, 2001, **63**, 075406.
51 A. Barbieri, M. A. Van Hove and G. A. Somorjai, *Surf. Sci.*, 1994, **306**, 261.
52 H. Ohtani, M. A. V. Hove and G. A. Somorjai, *Surf. Sci.*, 1987, **187**, 372.
53 Y. B. He, A. Stierle, W. X. Li, A. Farkas, N. Kasper and H. Over, *J. Phys. Chem. C*, 2008, **112**, 11946.
54 S. Schwegmann, H. Over, V. De Renzi and G. Ertl, *Surf. Sci.*, 1997, **375**, 91.
55 M. E. Grillo, C. Stampfl and W. Berndt, *Surf. Sci.*, 1994, **317**, 84.
56 D. L. Adams, H. B. Nielsen and M. A. Van Hove, *Phys. Rev. B: Condens. Matter*, 1979, **20**, 4789.
57 M. Gajdoš, A. Eichler and J. Hafner, *J. Phys.: Condens. Matter*, 2004, **16**, 1141.
58 H. B. Michaelson, *J. Appl. Phys.*, 1977, **48**, 4729.
59 P. Brault, H. Range, J. P. Toennies and C. Woll, *Z. Phys. Chem.*, 1997, **198**, 1.
60 J. E. Demuth, *Chem. Phys. Lett.*, 1977, **45**, 12.
61 G. B. Fisher, *Chem. Phys. Lett.*, 1981, **79**, 452.
62 R. Gomer, *Acc. Chem. Res.*, 1996, **29**, 284.
63 G. N. Derry and J.-Z. Zhang, *Phys. Rev. B: Condens. Matter*, 1989, **39**, 1940.
64 Y. Jia, B. Wu, H. H. Weitering and Z. Y. Zhang, *Phys. Rev. B: Condens. Matter Mater. Phys.*, 2006, **74**, 035433.
65 Z.-H. Zeng, J. L. F. Da Silva and W.-X. Li*Phys. Rev. B: Condens. Matter Mater. Phys.*, accepted.
66 P. J. Feibelman, B. Hammer, J. K. Nørskov, F. Wagner, M. Scheffler, R. Stumpf, R. Watwe and J. Dumesic, *J. Phys. Chem. B*, 2001, **105**, 4018.
67 Y. Wang, S. de Gironcoli, N. S. Hush and J. R. Reimers, *J. Am. Chem. Soc.*, 2007, **129**, 10402.
68 K. Doll, *Surf. Sci.*, 2004, **573**, 464.
69 S. E. Mason, I. Grinberg and A. M. Rappe, *Phys. Rev. B: Condens. Matter Mater. Phys.*, 2004, **69**, 161401.
70 G. Kresse, A. Gil and P. Sautet, *Phys. Rev. B: Condens. Matter Mater. Phys.*, 2003, **68**, 073401.
71 A. Gil, A. Clotet, J. M. Ricart, G. Kresse, M. Garcia-Hernandez, N. Rosch and P. Sautet, *Surf. Sci.*, 2003, **530**, 71.
72 Q. M. Hu, K. Reuter and M. Scheffler, *Phys. Rev. Lett.*, 2007, **98**, 176103.
73 M. Neef and K. Doll, *Surf. Sci.*, 2006, **600**, 1085.
74 M. Gajdoš and J. Hafner, *Surf. Sci.*, 2005, **590**, 117.
75 M. Alaei, H. Akbarzadeh, H. Gholizadeh and S. de Gironcoli, *Phys. Rev. B: Condens. Matter Mater. Phys.*, 2008, **77**, 085414.
76 A. Stroppa and G. Kresse, *New J. Phys.*, 2008, **10**, 063020.
77 A. L. Allred, *J. Inorg. Nucl. Chem.*, 1961, **17**, 215.
78 L. D. Schmidt and R. Gomer, *J. Chem. Phys.*, 1966, **45**, 1605.
79 W. X. Li, C. Stampfl and M. Scheffler, *Phys. Rev. B: Condens. Matter Mater. Phys.*, 2002, **65**, 075407.
80 A. Michaelides, P. Hu, M. H. Lee, A. Alavi and D. A. King, *Phys. Rev. Lett.*, 2003, **90**, 246103.

Downloaded by Dalian Institute of Chemical Physics, CAS on 02/05/2013 07:43:48.
Published on 26 January 2010 on http://pubs.rsc.org | doi:10.1039/B920857G

 This journal is © the Owner Societies 2010